Advanced Synthesis & Catalysis

FULL PAPERS

DOI: 10.1002/adsc.201500239

Expanding Substrate Specificity of ω-Transaminase by Rational Remodeling of a Large Substrate-Binding Pocket

Sang-Woo Han,[a] Eul-Soo Park,[a] Joo-Young Dong,[a] and Jong-Shik Shin[a,*]

[a] Department of Biotechnology, Yonsei University, Shinchon-Dong 134, Seodaemun-Gu, Seoul 120-749, South Korea
Fax: (+82)-2-362-7265; phone: (+82)-2-2123-5884; e-mail: enzymo@yonsei.ac.kr

Received: March 10, 2015; Revised: May 29, 2015; Published online: August 13, 2015

Supporting information for this article is available on the WWW under http://dx.doi.org/10.1002/adsc.201500239.

Abstract: Production of structurally diverse chiral amines *via* biocatalytic transamination is challenged by severe steric interference in a small active site pocket of ω-transaminase (ω-TA). Herein, we demonstrated that structure-guided remodeling of a large pocket by a single point mutation, instead of excavating the small pocket, afforded desirable alleviation of the steric constraint without deteriorating parental activities toward native substrates. Molecular modeling suggested that the L57 residue of the ω-TA from *Ochrobactrum anthropi* acted as a latch that forced bulky substrates to undergo steric interference with the small pocket. Removal of the latch by a L57A substitution allowed relocation of the small pocket and dramatically improved activities toward various arylalkylamines and alkylamines (e.g., 1100-fold increase in k_{cat}/K_M for α-propylbenzylamine). This approach may provide a facile strategy to broaden the substrate specificity of ω-TAs.

Keywords: chiral amines; molecular modeling; protein engineering; substrate specificity; ω-transaminase

Introduction

Chiral amines serve as essential structural elements found in a number of pharmaceutical drugs, agrochemicals and chiral ligands.[1] Recent research efforts to realize industrial exploitation of ω-transaminase (ω-TA) have been spurred by the unique catalytic performance of ω-TA enabling reversible stereoselective transfer of an amino group between primary amines and carbonyl compounds using pyridoxal 5′-phosphate (PLP) as a prosthetic group (Scheme 1).[2] ω-TA affords biocatalytic routes to the production of enantiopure amines *via* kinetic resolution of racemic amines[3] as well as asymmetric amination of prochiral ketones.[2c,4]

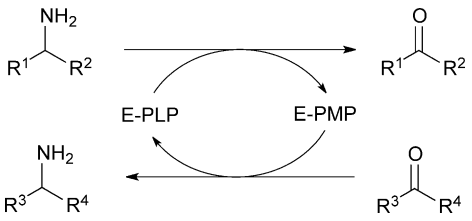

Scheme 1. Schematics of the ω-TA reaction. Transfer of an amino group is mediated by interconversion between an enzyme-PLP form (E-PLP) and a pyridoxamine 5′-phosphate (PMP) form of the enzyme (E-PMP).

Despite several enzymatic properties of ω-TA beneficial for industrial applications such as stringent stereoselectivity, high turnover rate and no requirement for an external cofactor, preparation of structurally diverse amines has been challenged by strictly defined constraints in the substrate-binding pockets of the enzyme.[2b,5] We previously proposed an active site model of ω-TA, consisting of two differently sized active site pockets.[6] Substrate specificities of both (*S*)- and (*R*)-selective ω-TAs are consistent with the two-binding-site model where key structural determinants cause severe steric interference in a small (S) pocket, precluding entry of substituents larger than an ethyl group, and dual recognition of hydrophobic and carboxyl groups in a large (L) pocket.[6,7] The steric constraint in the S pocket has been identified as a crucial limiting factor to the production of diverse chiral amines. To date, the only exception to the strict steric constraint in the S pocket has been reported with an (*S*)-selective ω-TA cloned from *Paracoccus denitrificans* (PDTA) which readily accepts α-keto acids carrying side chains up to a *n*-butyl group.[8] However, the non-canonical steric constraint of PDTA was not

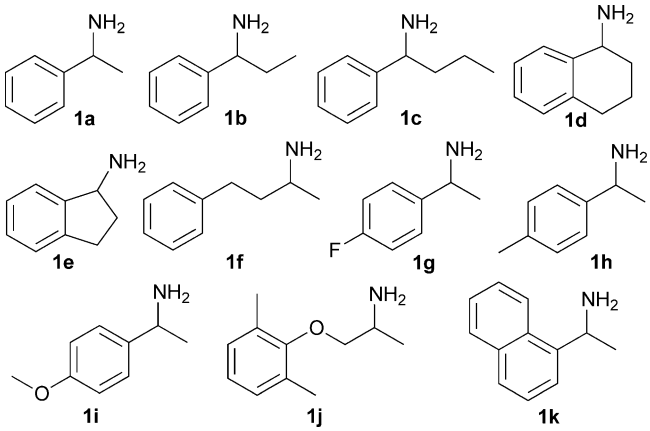

Scheme 2. Chiral arylalkylamines used in this study.

observed with the arylalkylamines listed in Scheme 2.[8]

To expand the substrate range of naturally occurring ω-TAs, it is highly desirable to construct an engineered variant displaying a relaxed steric constraint in the S pocket. In this regard, we previously showed that a single point mutation of a small-pocket-forming residue of PDTA substantially improved activity for (*S*)-**1c**.[8] Another example to engineer an (*S*)-selective ω-TA was reported by Midelfort et al., which employed multiple mutations of an ω-TA from *Vibrio fluvialis* for asymmetric synthesis of a β-amino ester (i.e., imagabalin).[9] The same ω-TA was also engineered elsewhere to improve activities toward α-hydroxy ketones and aryl alkyl ketones, which employed structure-guided partial saturation mutagenesis.[10] Very recently, engineering of an ω-TA from *Chromobacterium violaceum* was demonstrated to improve the activity for L-serine.[11] The most successful demonstration dealt with protein engineering of an (*R*)-selective ω-TA from *Arthrobacter* sp. (ARTA) to prepare a bulky chiral amine (i.e., sitagliptin) from a ketone precursor.[2c] In the case of the engineered ARTA ($AR_{mut}TA$), multiple mutations accumulated during iterative rounds of directed evolution led to the sacrifice of a beneficial parental property. We found that $AR_{mut}TA$ showed substantial activity decreases for amine substrates such as (*R*)-**1a** and (*R*)-**1e** (i.e., 7 and 65% residual activities, respectively, relative to ARTA), seemingly in compensation for 4-, 56- and 25-fold activity increases toward (*R*)-**1b–d**, respectively (Table S1 in the Supporting Information).

In this study, we tackled engineering of the substrate specificity of the (*S*)-selective ω-TA from *Ochrobactrum anthropi* (OATA) because the enzyme displays exceptionally high activity toward isopropylamine[12] which is an ideal amino donor for asymmetric amination of ketones.[2c,4c,13] We aimed at creating an OATA variant displaying broad substrate specificity without losing activities toward native substrates such as (*S*)-**1a** and isopropylamine by introducing a minimal modification to the parental enzyme.[14]

Results and Discussion

Molecular Modeling of the Active Site of OATA

Similarly to other ω-TAs, the S pocket of OATA showed severe steric interference when accepting substituents bulkier than a methyl group. Compared with (*S*)-**1a**, the relative reactivities of (*S*)-**1b–d** were only 1.9, 0.2 and 2.5%, respectively.[15] To identify key residues responsible for the steric interference, we performed homology modeling and substrate docking simulation. Note that $AR_{mut}TA$ could not be used as a reference to identify the key residues of OATA because (*S*)- and (*R*)-selective ω-TAs are evolutionarily distant and belong to different fold classes.[16] A structural model of the homodimeric OATA was constructed using X-ray structures of two well-characterized ω-TAs from *P. denitrificans* (PDB ID: 4GRX)[17] and *Chromobacterium violaceum* (4A6T),[18] and two recently discovered ω-TAs (3GJU and 3I5T)[19] as templates. To map the substrate binding pockets, we performed docking simulation with the homology model using (*S*)-**1a** as a ligand (Figure 1). For transaldimination to occur between an internal aldimine and an incoming amino donor, the amino group of the bound substrate should be proximal to the C-4′ of the PLP moiety.[8] In the docking model, the distance between

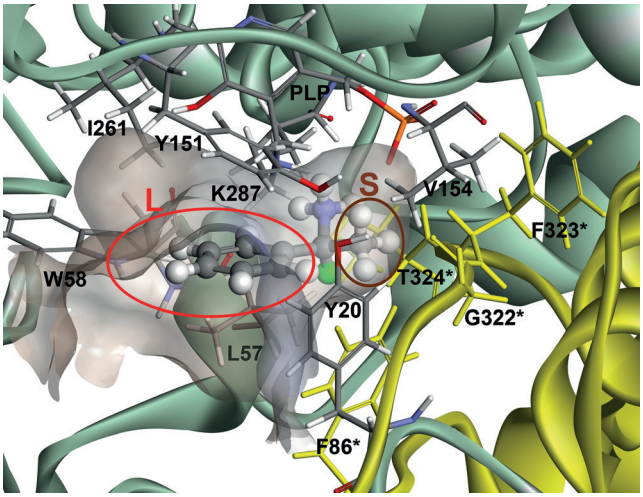

Figure 1. Docking model of (*S*)-**1a** in the active site of OATA. The active site is shown as a Connolly surface. The backbone chain and the amino acid residues coming from another subunit are colored in yellow. Ovals represent the L and S pockets. (*S*)-**1a**, whose C_α-hydrogen is colored in green, is shown in a ball-and-stick representation. K287 forms an internal aldimine with PLP.

the N of (*S*)-**1a** and the C-4′ was 2.9 Å which was slightly longer than that found with PDTA in the previous study (i.e., 2.3 Å).[8] It is notable that the C_α-hydrogen of (*S*)-**1a** points to the active site lysine (i.e., K287) to enable the hydrogen transfer required in a subsequent catalytic step.

The docking model predicts that the S pocket is surrounded by side chains of the five active site residues (i.e., Y20, F86*, Y151, V154 and T324*), a phosphate group of the PLP and a backbone chain ranging from G322* to T324*. Note that asterisks indicate the residues from another subunit. Consistent with the reactivities of (*S*)-**1a**–**d**, the S pocket is shaped to accept only up to a methyl substituent. The hydrophobic environment in the L pocket required to accommodate the phenyl group of (*S*)-**1a** seems to be provided by Y20, W58, F86* and Y151 that are conserved in the ω-TAs used as templates for the homology modeling (see the Supporting Information, Figure S1 for the sequence alignment).

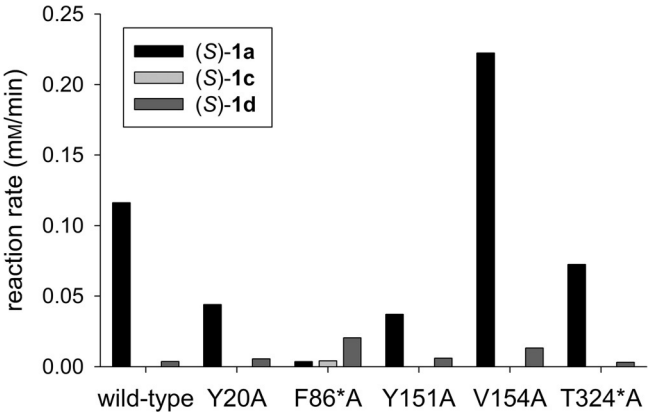

Figure 2. Alanine scanning mutagenesis of the five small-pocket-forming residues to examine relaxation of the steric interference. Reaction rate represents the initial rate per 1 μM enzyme and was measured at 10 mM (*S*)-amine and 10 mM pyruvate. Bars representing (*S*)-**1c** are not visible, except F86 A, due to too low reaction rates.

Mutations of the Small-Pocket-Forming Residues

Based on the agreement between the molecular modeling and the reactivities of (*S*)-**1a**–**d**, we set out to identify key residues responsible for the steric constraint in the S pocket. To this end, the five small-pocket-forming residues were individually substituted by alanine as we did previously with PDTA,[8] and activities of the resulting variants were measured against (*S*)-**1a** and (*S*)-**1c** and **d** (Figure 2). Alanine scanning mutagenesis of the three aromatic residues (i.e., Y20, F86* and Y151) led to large reductions in enzyme activity toward (*S*)-**1a**, presumably due to impairment of the hydrophobic environment required for recognition of the phenyl group of (*S*)-**1a**. In contrast, the activity decrease by a T324A mutation is ascribable to loss of a hydrogen bond between the amino group of (*S*)-**1a** and the hydroxy group of T324*. V154A mutation resulted in a 2-fold activity increase toward (*S*)-**1a**, suggesting that V154 contributes to the steric interference even with the methyl group of (*S*)-**1a**. This result is in line with the 2.7-fold higher activity of the wild-type OATA toward benzylamine, the hydrogen of which enters the S pocket, compared with that toward (*S*)-**1a**.[20] Although the V154A substitution enhanced activities toward (*S*)-**1a** as well as (*S*)-**1d**, relaxation in the steric constraint was not large enough to permit a detectable activity increase toward (*S*)-**1c**. Among the alanine mutants, F86A was the only one affording substantial activity improvement for (*S*)-**1c**, along with the highest fold-increase in the reactivity of (*S*)-**1d** (i.e., 3.7-fold). However, a drastic loss in the activity toward (*S*)-**1a** deterred us to carry out further engineering of the F86A variant.

The alanine scanning mutagenesis indicated that F86* and V154 were hot spots for excavating the S pocket. Thus, a plausible strategy to relieve the steric constraint might be selection of a promising hit from a library carrying multiple mutations including the hot spots and then iterative mutations elsewhere until reaching a desirable activity.[2c,21] However, a technical challenge in the excavation-based strategy is that the small-pocket-forming residues directly contact the phosphate group of the catalytically important PLP and participate in the subunit-subunit interface (Figure 1). Therefore, excavation of the S pocket without damaging catalytic turnover and enzyme stability would be a challenging task requiring massive mutations. In contrast, the L pocket is secluded from the PLP and the subunit interface. These structural features of the active site led us to explore the possibility as to whether a mutation in the L pocket could induce different substrate binding that allowed bulky substituents to be accommodated in a less hindered region rather than in the native S pocket.

Rational Remodeling of the L Pocket

To implement the binding-pocket relocation concept, we scrutinized the docking model and realized that L57 and Y151 play a key role in the steric constraint because intercalation of the phenyl group between them forced the methyl group of (*S*)-**1a** to be directed to the S pocket (Figure 3A). While the aromatic ring of Y151 is juxtaposed with the phenyl substituent of (*S*)-**1a**, the alkyl side chain of L57 partially contacts the bottom side of the phenyl group. Therefore, L57 seems to function as a latch that confines the phenyl group next to Y151. This led us to envisage that re-

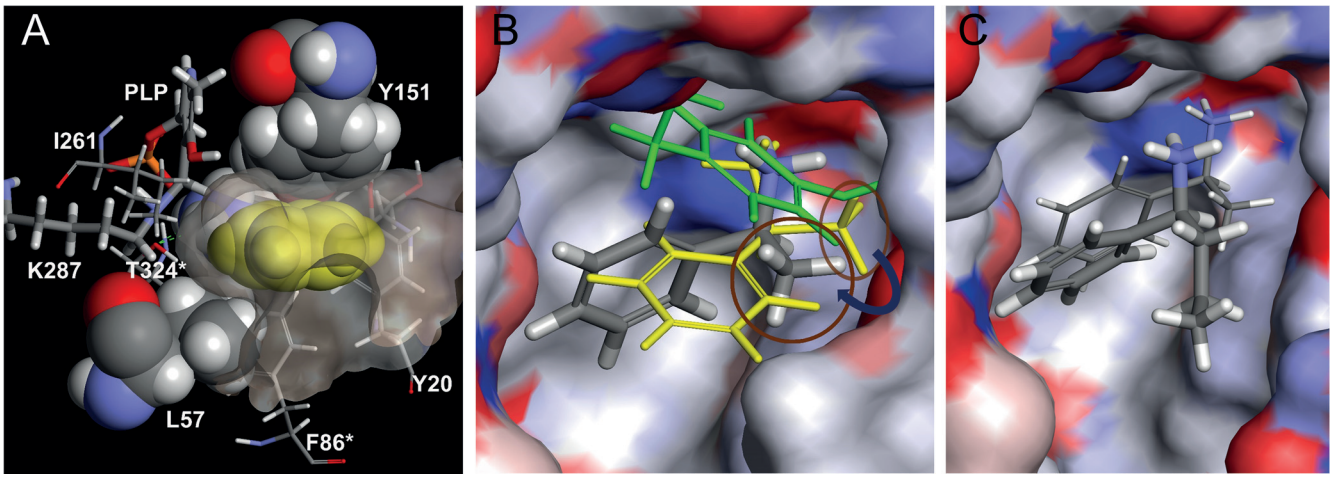

Figure 3. Structure-guided relocation of the S pocket by engineering the L pocket. (**A**) A side view of Figure 1 to visualize intercalation of the phenyl group of (*S*)-**1a** (colored in yellow) between L57 and Y151 that are shown as a CPK representation. The active site is shown as a Connolly surface. Green dotted lines represent hydrogen bonds between T324* and the amino group of (*S*)-**1a**. The internal aldimine is shown as thick sticks. (**B**) Docking model of (*S*)-**1a** in the L57A variant. Yellow sticks represent the docking pose of (*S*)-**1a** in the wild-type OATA. Blue arrow represents the relocation of the S pocket. Green sticks represent Y151. (**C**) Docking model of (*S*)-**1c** in the L57A variant. Thin sticks represent the docking pose of (*S*)-**1a** in the L57A variant. To clearly visualize the propyl group of (*S*)-**1c**, the Connolly surface of the active site excludes P165 which is shown as a bump in the right bottom of Figure 3B. Y151 is also omitted for a clear representation of the bound substrate.

moval of the latch could unleash the phenyl group and thereby enable the methyl group to move to a spacious region from the native S pocket. We performed molecular modeling to examine whether substitution of L57 with a smaller residue could induce the desirable S pocket relocation. Docking simulation with (*S*)-**1a** suggested that L57V mutation failed to remove the latch (Supporting Information, Figure S2). In contrast, L57A mutation was predicted to enable the phenyl group to be positioned perpendicular to Y151 and thus the methyl group to escape from the native S pocket with a slight increase in the N-to-C-4′ distance (i.e., 3.2 Å) (Figure 3B). Moreover, the remodeled L pocket was predicted to allow productive binding of (*S*)-**1c** (i.e., the N-to-C-4′ distance of 3.4 Å) by letting the propyl group point to a solvent side (Figure 3C). In contrast, consistent with the activity data shown in Figure 2, (*S*)-**1c** failed to form a productive binding to the active site of the wild-type OATA (i.e., the N-to-C-4′ distance of 5.7 Å as shown in the Supporting Information, Figure S3).

Activity Improvements toward Arylalkylamines

Motivated by the molecular modeling results, we constructed the L57A variant and examined activities toward arylalkylamines in comparison with the parental enzyme (Table 1). Indeed, the L57A variant showed dramatic activity improvements toward substrates carrying bulky alkyl substituents bonded to a C_α carbon (i.e., 19-, 150-, 30- and 7-fold activity increases toward (*S*)-**1b–e**, respectively). However, the L57V mutation did not elicit such activity improvements toward (*S*)-**1b** and **c** (Supporting Information, Table S2), consistent with the modeling result. Moreover, the L57A mutation led to substantial activity in-

Table 1. Activity improvements of OATA by the L57A substitution toward arylalkylamines.

Amines	Relative reactivity[a] [%]		Fold-increase
	wild-type	L57A	
(*S*)-**1a**	100.0[b]	141.0	1.4
(*S*)-**1b**	1.9	36.6	19
(*S*)-**1c**	0.2	30.0	150
(*S*)-**1d**	2.5	74.9	30
(*S*)-**1e**	10.9	72.1	7
(*S*)-**1f**	89.1	165.2	1.9
(*S*)-**1g**	37.8	121.3	3.2
(*S*)-**1h**	86.1	192.7	2.2
(*S*)-**1i**	115.5	119.5	1.0
(*S*)-**1j**	33.3	74.6	2.2
(*S*)-**1k**	0.3	19.8	66
benzylamine	273.4	687.2	2.5

[a] Relative reactivity represents the initial reaction rate (i.e., conversion <10%) normalized by that of (*S*)-**1a** measured with the wild-type enzyme. Reaction conditions were 50 mM amine, 50 mM pyruvate and 2 μM ω-TA. In the case of **1f**, **1g** and **1j**, 100 mM racemic amine were used in the rate measurements.

[b] Initial reaction rate was 455 μM min^{-1}.

Table 2. Activity improvements of the L57A variant toward alkylamines.

	R	Relative reactivity[a] [%] wild-type	L57A	Fold-increase
isopropylamine	$-CH_3$	24.8	32.2	1.3
(*S*)-**2a**	$-CH_2CH_3$	35.3	139.8	4.0
(*S*)-**2b**	$-(CH_2)_2CH_3$	15.4	71.8	4.7
(*S*)-**2c**	$-(CH_2)_3CH_3$	37.8	124.5	3.3
(*S*)-**2d**	$-(CH_2)_5CH_3$	177.7	318.3	1.8
(*S*)-**2e**	$-CH(CH_3)_2$	22.0	114.9	5.2
(*S*)-**2f**	$-CH_2CH(CH_3)_2$	3.5	16.5	4.8
(*S*)-**2g**	-cyclopropyl	35.7	129.2	3.6
(*S*)-**2h**	$-CH_2OCH_3$	35.3	52.0	1.5

[a] Relative reactivity represents the initial reaction rate normalized by that of (*S*)-**1a** measured with the wild-type OATA. Reaction conditions were 50 mM amine, 50 mM pyruvate and 2 μM ω-TA. In the case of **2b**, **2e**, **2f** and **2h**, 100 mM racemic amine were used in the rate measurements.

creases toward the amines carrying a methyl substituent bonded to a C_α carbon [i.e., (*S*)-**1a** and (*S*)-**1f–k**], seemingly owing to altered binding of the bulky arylalkyl substituents to the remodeled L pocket that permitted the methyl substituent to be placed in a less hindered region. Notably, (*S*)-**1k** carrying a naphthyl substituent [0.3% parental reactivity relative to (*S*)-**1a**] turned into a reactive substrate with a 66-fold reactivity increase. Interestingly, the enhanced activity of the L57A variant was also observed with benzylamine, suggesting that even a hydrogen can undergo steric interference in the S pocket of the wild-type enzyme.

Activity Improvements toward Alkylamines

The activity improvements against various arylalkylamines by the L pocket remodeling led us to examine whether the L57A variant would also exhibit improved activities toward amine substrates of which the alkyl substituents, instead of the arylalkyl ones, took up the L pocket (Table 2). Note that the alkylamines listed in Table 2 carry a methyl group bonded to a C_α carbon like the arylalkylamines such as **1a** and **1f–k**. Similarly to the activity improvements observed with (*S*)-**1a** and (*S*)-**1f–k**, the L57A variant showed marked activity increases for all the alkylamines tested. Highest reactivity increases were observed with the alkylamines carrying branched alkyl substituents such as (*S*)-**2e** and **f** (i.e., 5.2- and 4.8-fold increases, respectively). It is notable that the L57A mutation substantially improved activity toward isopropylamine. Taken together, the L57A variant seems to afford the S pocket relocation irrespective of the type of substituent placed in the L pocket.

Activity Improvements toward Aryl Alkyl Ketones

To examine synthetic utility of the L57A variant for asymmetric amination of ketones, we measured activities for six aryl alkyl ketones (Table 3). The L57A variant was found to retain the high enantioselectivity of the wild-type enzyme, because both enzymes afforded synthesis of (*S*)-amines in over 99% *ee*. Consistent with the activity improvements toward (*S*)-**1b** and **c**, the L57A variant afforded marked activity increases for the aryl alkyl ketones carrying alkyl substituents larger than a methyl group (i.e., 8. and 110-fold reactivity increases for **3b** and **3c**, respectively). Moreover, we observed modest activity improvements for **3e** and **f** which carry sterically less demanding substituents for the S pocket. However, **3d** remained inert for the L57A variant. Despite the high activity improvement

Table 3. Effect of the L57A mutation on the activity improvements toward aryl alkyl ketones.[a]

Ketone		Reaction rate ($\mu M\,min^{-1}$)[b] wild-type	L57A	Fold-increase
3a	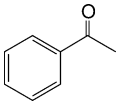	0.17 (>99)[c]	0.15 (>99)	0.88
3b	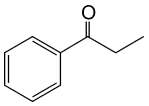	9.6×10^{-4} (>99)	8.0×10^{-3} (>99)	8
3c	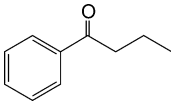	3.0×10^{-5} (>99)	3.2×10^{-3} (>99)	110
3d	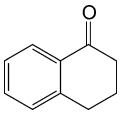	n.d.[d]	n.d.	–
3e	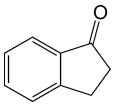	9.0×10^{-4} (>99)	1.1×10^{-3} (>99)	1.22
3f	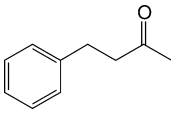	0.52 (>99)	0.74 (>99)	1.42

[a] *Reaction conditions:* 50 mM ketone, 500 mM isopropylamine and 0.1 mM PLP in phosphate buffer (50 mM, pH 7) containing 15% v/v DMSO at 37 °C.
[b] Reaction rate represents the initial rate per 1 μM enzyme.
[c] Values in the parenthesis represent *ee* of the produced (*S*)-amines.
[d] n.d.: not detectable.

Table 4. Kinetic parameters for arylalkylamines.[a]

Amine	Wild-type			L57A			Fold-increase in k_{cat}/K_M
	K_M [mM]	k_{cat} [s^{-1}]	k_{cat}/K_M [M^{-1} s^{-1}]	K_M [mM]	k_{cat} [s^{-1}]	k_{cat}/K_M [M^{-1} s^{-1}]	
(*S*)-**1a**	130	20	150	54	18	330	2
(*S*)-**1b**	160	0.19	1.2	91	2.8	31	26
(*S*)-**1c**	690	0.010	0.014	200	3.1	16	1100
(*S*)-**1d**	86	0.36	4.2	20	4.2	210	50
(*S*)-**1e**	430	4.3	10	18	4.3	240	24

[a] Kinetic parameters represent apparent rate constants determined at a fixed concentration of pyruvate (20 mM).

for **3c** induced by the L57A mutation, the actual activity of the L57A variant for **3c** was only 2% relative to that of the wild-type for **3a**. Taken together, the L57A mutation does not provide desirable improvement in the catalytic performance required for practical amination of aryl alkyl ketones although the variant is highly promising for kinetic resolution of the bulky chiral amines.

Kinetic Analysis of the L57A Variant

To gain insights into how the L57A mutation affected binding and catalytic turnover, we performed kinetic analyses with (*S*)-**1a**-.**e** (Table 4). As expected, all the amines showed enhanced binding to the remodeled active site (i.e., decreases in K_M). In contrast to (*S*)-**1a** and (*S*)-**1e**, turnover rates (k_{cat}) of (*S*)-**1b**–**d** were greatly accelerated. These results suggest that the three amines, which show very low reactivities with the wild-type enzyme, undergo relaxation in the steric interference by the active site remodeling throughout the binding and catalytic steps, leading to dramatic increases in the specificity constant (k_{cat}/K_M) as observed with (*S*)-**1c** (i.e., 1100-fold increase). It is notable that the L57A variant showed 24-fold increase in k_{cat}/K_M for (*S*)-**1e** while $AR_{mut}TA$ showed 35% reduction in the activity toward (*R*)-**1e** (Supporting Information, Table S1).

Kinetic Resolution of *rac*-1c

To demonstrate synthetic utility of the L57A variant, we compared catalytic performances of the wild-type and the L57A variant in the kinetic resolution of *rac*-**1c** (Figure 4). The L57A variant afforded 99.6% *ee* of (*R*)-**1c** at 50.4% conversion after 20 h, whereas the wild-type enzyme led to only 3.6% *ee* and 3.9% conversion. Based on this result, enantioselectivity (*E*) of the L57A variant for **1c** was estimated to be >200.[22] Taken together with the >99% *ee* of the (*S*)-amines synthesized from ketones as shown in Table 3, this result indicates that the L57A mutation does not affect the stringent enantioselectivity of the wild-type enzyme at all.

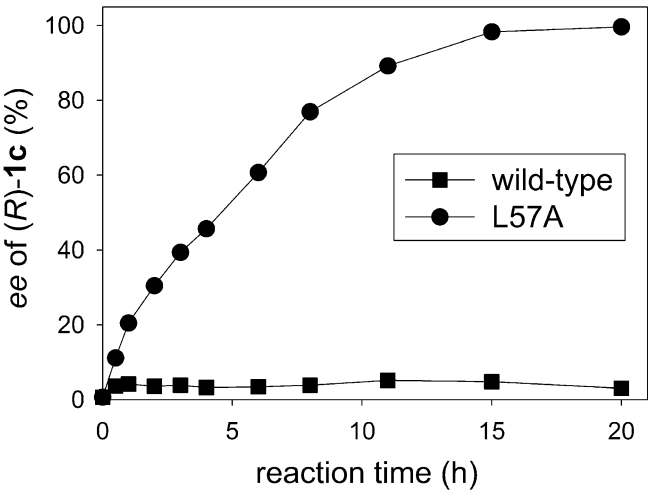

Figure 4. Comparison of the kinetic resolution of *rac*-**1c** using the wild-type OATA and the L57A variant. Reaction conditions were 100 mM *rac*-**1c**, 100 mM glyoxylate and 40 μM enzyme in phosphate buffer (50 mM, pH 7) at 37 °C.

The high *E* value of the L57A variant led us to carry out a preparative-scale kinetic resolution of **1c** in a 50-mL reaction mixture charged with *rac*-**1c** (1.12 g, 150 mM), glyoxylic acid (0.56 g, 150 mM) and L57A OATA (80 μM). After 30 h reaction, *ee* of (*R*)-**1c** reached 99.7% at 50.9% conversion. The resulting reaction mixture was subjected to product isolation and structural characterization, leading to recovery of pure (*R*)-**1c** (0.48 g, 86% isolation yield, 99.7% *ee*).

Asymmetric Synthesis of (*S*)-1c

To examine how the activity improvement for **3c** induced by the L57A mutation benefits asymmetric synthesis of (*S*)-**1c**, we carried out ω-TA reactions starting with 4.2 mM **3c** and 300 mM isopropylamine. The L57A variant afforded the synthesis of 3.3 mM (*S*)-**1c** (i.e., 79% conversion) with >99% *ee* at 3 days, whereas the wild-type OATA led to no detectable accumulation of (*S*)-**1c** until 4 days. The synthesis reac-

tion using the L57A variant showed no further increase in the conversion after 3 days, which led us to presume that the reaction reached an equilibrium state at 3 days. Indeed, the equilibrium concentration of (*S*)-**1c** at the given reaction conditions is calculated to be 3.5 mM by assuming that the equilibrium constant for the reaction between **3c** and isopropylamine can be approximated to that between **1c** and isopropylamine (i.e., 0.06).[23]

Implications to the S Pocket Engineering of ω-TA

Recently, X-ray structures of two (*R*)-selective ω-TAs have been released.[24] We performed docking simulation of (*R*)-**1a** in the active site of the ω-TA from *Aspergillus terreus* (47% sequence identity to ARTA) to identify structural differences in the active sites of the (*R*)- and (*S*)-selective ω-TAs (Supporting Information, Figure S4). We found that locations of the L and S pockets of the *A. terreus* ω-TA were exactly opposite to those of OATA when the amino group and the C_α-hydrogen of (*R*)-**1a** were overlaid on those of (*S*)-**1a** in Figure 1, which makes sense considering the opposite stereoselectivity of the two ω-TAs. Interestingly, the L pocket of the *A. terreus* ω-TA was found on the subunit-subunit interface while the S pocket was located distal to the interface. Therefore, the S pocket seems to be amenable to engineering, which underlined the excavation-based strategy demonstrated with ARTA by Savile et al.[2c] However, application of the same strategy to (*S*)-selective ω-TAs should be challenged by malfunctioning of catalytic turnover and structural stability owing to the proximity of the S pocket to the subunit interface as we observed with alanine scanning mutagenesis of the small pocket residues of OATA. Thus, massive mutations would be required to counteract the adverse mutational effects. This explains why the S pocket excavation to accept bulky amine substrates has been difficult with (*S*)-selective ω-TAs in spite of their much earlier discovery and broader natural occurrence than the (*R*)-selective ones.[1b,2b,5]

Conclusions

In this study, we aimed at engineering the substrate specificity of OATA by alleviating the steric constraint in the S pocket without sacrificing beneficial native activities. Instead of excavating the S pocket which was hard to be engineered, we rationally remodeled the L pocket by a single point mutation to induce altered substrate binding that allowed a less hindered region to be adopted as a new S pocket. The S pocket relocation strategy was successful in expanding the substrate specificity toward various arylalkylamines and alkylamines.

Experimental Section

Chemicals

(*S*)-1-Phenylbutylamine [(*S*)-**1c**] was purchased from Alfa Aesar (Ward Hill, USA). Pyruvic acid was obtained from Kanto Chemical Co. (Tokyo, Japan). Isopropylamine was purchased from Junsei Chemical Co. (Tokyo, Japan). All other chemicals were purchased from Sigma Aldrich Co. (St. Louis, USA) and of the highest grade available. Materials used for preparation of culture media including yeast extract, tryptone and agar were purchased from Difco. (Spark, USA).

Overexpression and Purification of Transaminases

Preparation of the His_6-tagged OATA was carried out as described elsewhere with minor modifications.[25] *Escherichia coli* BL21(DE3) cells transformed with pET28a(+) expression vectors harboring the OATA gene were cultivated at 37 °C in LB medium containing 50 μg mL^{-1} kanamycin. At around 0.6 OD_{600}, protein expression was induced by IPTG (1 mM) and the cells were allowed to grow for 10 h. Cells were harvested and disrupted by an ultrasonicator. Protein purification was carried out on ÄKTAprime plus (GE Healthcare, USA) using a HisTrap HP column (GE Healthcare) and a HiTrap desalting column (GE Healthcare). When necessary, the enzyme solution was concentrated using an ultrafiltration kit (Ultracel-30) purchased from Millipore Co. (Billerica, USA). UV absorbance of the purified enzyme solution was measured at 280 nm, which was used to calculate the molar enzyme concentration using an extinction coefficient of OATA (i.e., 78,076 M^{-1} cm^{-1}).

Enzyme Assay

Unless otherwise specified, enzyme assays were carried out at 37 °C and pH 7 (50 mM phosphate buffer). One unit of OATA activity was defined as the enzyme amount that catalyzes the formation of 1 μmol of acetophenone in 1 min at 10 mM pyruvate and 10 mM (*S*)-**1a**. Typical reaction volume was 100 μL and the enzyme reaction was stopped after 10 min by adding 600 μL acetonitrile. For initial rate measurements, acetophenone was analyzed by HPLC.

Site-Directed Mutagenesis

Variants of OATA carrying a single point mutation were created by a QuikChange Lightning site-directed mutagenesis kit (Stratagene) according to the instruction manual. Mutagenesis primers, listed in the Supporting Information, Table S3, were designed using a primer design program (http://www.stratagene.com). The template used for the mutagenesis PCR was pET28-OATA which was previously constructed.[26] Intended mutagenesis was confirmed by DNA sequencing.

Molecular Modeling

Molecular modeling simulations were performed with the Discovery Studio package (version 3.5.0, Accelrys, USA) using the CHARMm force field. A homology model of OATA was built using the Modeler module (version 9.8). X-ray structures of the four ω-TAs from *P. denitrificans* (PDB ID: 4GRX), *C. violaceum* (4A6T), *Mesorhizobium loti* (3GJU) and *Rhodobacter sphaeroides* (3I5T) were used as templates. Sequence alignment for the homology modeling was carried out using BLOSUM62 as a scoring matrix with a default setting (−900 gap open penalty; −50 gap extension penalty). To generate a holoenzyme structure, PLP was copied from 4A6T and transferred into the homology model. Ramachandran phi-psi analysis showed that 0.4% non-glycine residues lay in the disallowed region, indicative of the validity of the homology model.

Active site models of OATA variants were constructed by amino acid substitution on the homology model of the wild-type OATA, followed by energy minimization of the mutation site until the RMS gradient reached 0.1 kcal mol^{-1} Å. Docking simulations using (*S*)-**1a** and (*S*)-**1c** as ligands were accomplished using the CDOCKER module under a default setting (2,000 steps at 700 K for a heating step; 5,000 steps at 300 K for a cooling step; 8 Å grid extension) within the active site defined by the Binding-Site module.

Substrate Specificity

To examine substrate specificity, initial reaction rates were measured. Conversions were less than 10% in the initial rate measurements which were independently triplicated. Reaction conditions to measure activities of the five alanine mutants toward (*S*)-**1a**, (*S*)-**1c** and (*S*)-**1d** were 10 mM (*S*)-amine and 10 mM pyruvate in 50 mM phosphate buffer (pH 7.0) at 37 °C. Produced ketones (i.e., acetophenone, butyrophenone and α-tetralone) were analyzed by HPLC.

To measure amino donor reactivities of various arylalkylamines and alkylamines, (*S*)-amine (50 mM) and pyruvate (50 mM) were used as substrates and the L-alanine produced was analyzed by HPLC. In the case of **1f**, **1g**, **1j**, **2b**, **2e**, **2f** and **2h**, 100 mM racemic amine were used in the rate measurements. In the case of benzylamine and isopropylamine, 50 mM were used. Amino acceptor reactivities of aryl alkyl ketones were measured by HPLC analyses of the produced (*S*)-amines after derivatization with the Marfey's reagent.

Kinetic Measurements and Analysis

To obtain apparent kinetic parameters, a pseudo-one-substrate kinetic model was used under the fixed concentration of the cosubstrate.[27] To determine rate constants of arylalkylamines, varying concentrations of (*S*)-amine (i.e., 10–400 mM) at 20 mM pyruvate were used for the initial rate measurements. Produced ketone [i.e., acetophenone, propiophenone, butyrophenone, α-tetralone and 1-indanone for (*S*)-**1a**–**e**, respectively] was analyzed by HPLC. The initial rate data were fitted to a Michaelis–Menten equation, and the K_M and k_{cat} values were calculated from the slopes and y-intercepts of the double reciprocal plots.

Kinetic Resolution of *rac*-1c

Reaction conditions for the small-scale kinetic resolution of *rac*-**1c** were 100 mM *rac*-**1c**, 100 mM glyoxylate, 0.1 mM PLP and 40 μM ω-TA (i.e. 24 U/mL wild-type or 20 U/mL L57A variant) in 50 mM phosphate buffer (pH 7) at 37 °C. Total reaction volume was 1 mL. At predetermined reaction times, aliquots of the reaction mixture were sampled and subjected to quantitative chiral analysis of **1c** by HPLC.

Preparative-scale kinetic resolution of *rac*-**1c** was carried out at 37 °C under magnetic stirring in an oven-dried beaker charged with 50 mL reaction mixture containing *rac*-**1c** (7.5 mmol), glyoxylic acid (7.5 mmol), PLP (5 μmol), L57 A OATA (4 μmol) and potassium phosphate (50 mM, pH 7.0). When the enantiomeric excess of (*R*)-**1c** exceeded 99%, the reaction mixture was subjected to product isolation.

Asymmetric Synthesis of (*S*)-1c

Reaction conditions for the synthesis of (*S*)-**1c** were 4.2 mM **3c**, 300 mM isopropylamine, 1 mM PLP and 500 μM ω-TA in 50 mM Tris buffer (pH 7) containing 15% DMSO. Total reaction volume was 0.6 mL and the reaction was carried out at 37 °C. Fifty μL of the reaction mixture was sampled every 24 h until 4 days.

Isolation and Structural Characterization of (*R*)-1c

The pH of the reaction mixture was adjusted to 1.0 by adding 5 N HCl and then the resulting solution was filtered through a glass-fritted filter funnel to remove the protein precipitate. The filtrate solution was extracted with *n*-hexane (2×200 mL) to remove a trace amount of **3c**. The pH of the separated aqueous phase was adjusted to 12.0 by adding 10 N NaOH solution and then the resulting solution was extracted with *n*-hexane (2×200 mL). The organic extract was evaporated at 50 °C and 0.25 bar, leading to liquid (*R*)-**1c**. Structural characterization, including ^{1}H NMR, ^{13}C NMR, IR and LC/MS, was performed as described in the Supporting Information.

HPLC Analysis

HPLC analyses were performed on a Waters HPLC system (Waters Co., USA) or an YL9300 HPLC system (YL Instrument Co., South Korea). Analyses of aryl alkyl ketones were performed using a Symmetry column C18 (Waters Co.) as described elsewhere.[8] Quantitative chiral analyses of amines and L-alanine were carried out using the same HPLC column after chiral derivatization with 1-fluoro-2,4-dinitrophenyl-5-L-alanine amide (Marfey's reagent).[28] Details of the HPLC analyses are described in the Supporting Information.

Acknowledgements

We acknowledge financial support from the Advanced Biomass R&D Center (ABC-2011-0031358) through the National Research Foundation of Korea funded by the Ministry of Education, Science and Technology.

References

[1] a) T. C. Nugent, *Chiral Amine Synthesis: Methods, Developments and Applications*, Wiley-VCH, Weinheim, **2010**; b) U. T. Bornscheuer, G. W. Huisman, R. J. Kazlauskas, S. Lutz, J. C. Moore, K. Robins, *Nature* **2012**, *485*, 185–194; c) M. Breuer, K. Ditrich, T. Habicher, B. Hauer, M. Kesseler, R. Sturmer, T. Zelinski, *Angew. Chem.* **2004**, *116*, 806–843; *Angew. Chem. Int. Ed.* **2004**, *43*, 788–824; d) V. Gotor-Fernández, V. Gotor, *Curr. Opin. Drug Discovery Dev.* **2009**, *12*, 784–797.

[2] a) K. Hirotsu, M. Goto, A. Okamoto, I. Miyahara, *Chem. Rec.* **2005**, *5*, 160–172; b) D. Koszelewski, K. Tauber, K. Faber, W. Kroutil, *Trends Biotechnol.* **2010**, *28*, 324–332; c) C. K. Savile, J. M. Janey, E. C. Mundorff, J. C. Moore, S. Tam, W. R. Jarvis, J. C. Colbeck, A. Krebber, F. J. Fleitz, J. Brands, P. N. Devine, G. W. Huisman, G. J. Hughes, *Science* **2010**, *329*, 305–309; d) B. M. Nestl, S. C. Hammer, B. A. Nebel, B. Hauer, *Angew. Chem. Int. Ed.* **2014**, *53*, 3070–3095; e) M. Höhne, U. T. Bornscheuer, *ChemCatChem* **2009**, *1*, 42–51.

[3] a) P. Tufvesson, J. Lima-Ramos, J. S. Jensen, N. Al-Haque, W. Neto, J. M. Woodley, *Biotechnol. Bioeng.* **2011**, *108*, 1479–1493; b) R. L. Hanson, B. L. Davis, Y. Chen, S. L. Goldberg, W. L. Parker, T. P. Tully, M. A. Montana, R. N. Patel, *Adv. Synth. Catal.* **2008**, *350*, 1367–1375; c) M. Höhne, K. Robins, U. T. Bornscheuer, *Adv. Synth. Catal.* **2008**, *350*, 807–812.

[4] a) D. Koszelewski, I. Lavandera, D. Clay, G. M. Guebitz, D. Rozzell, W. Kroutil, *Angew. Chem.* **2008**, *120*, 9477–9480; *Angew. Chem. Int. Ed.* **2008**, *47*, 9337–9340; b) M. Höhne, S. Kühl, K. Robins, U. T. Bornscheuer, *ChemBioChem* **2008**, *9*, 363–365; c) K. E. Cassimjee, C. Branneby, V. Abedi, A. Wells, P. Berglund, *Chem. Commun.* **2010**, *46*, 5569–5571.

[5] M. S. Malik, E. S. Park, J. S. Shin, *Appl. Microbiol. Biotechnol.* **2012**, *94*, 1163–1171.

[6] J. S. Shin, B. G. Kim, *J. Org. Chem.* **2002**, *67*, 2848–2853.

[7] F. Steffen-Munsberg, C. Vickers, A. Thontowi, S. Schätzle, T. Meinhardt, M. S. Humble, H. Land, P. Berglund, U. T. Bornscheuer, M. Höhne, *ChemCatChem* **2013**, *5*, 154–157.

[8] E. S. Park, S. R. Park, S. W. Han, J. Y. Dong, J. S. Shin, *Adv. Synth. Catal.* **2014**, *356*, 212–220.

[9] K. S. Midelfort, R. Kumar, S. Han, M. J. Karmilowicz, K. McConnell, D. K. Gehlhaar, A. Mistry, J. S. Chang, M. Anderson, A. Villalobos, J. Minshull, S. Govindarajan, J. W. Wong, *Protein Eng. Des. Sel.* **2013**, *26*, 25–33.

[10] A. Nobili, F. Steffen-Munsberg, H. Kohls, I. Trentin, C. Schulzke, M. Höhne, U. T. Bornscheuer, *ChemCatChem* **2015**, *7*, 757–760.

[11] D. Deszcz, P. Affaticati, N. Ladkau, A. Gegel, J. M. Ward, H. C. Hailes, P. A. Dalby, *FEBS J.* **2015**, *282*, 2512–2436.

[12] E. S. Park, J. Y. Dong, J. S. Shin, *Org. Biomol. Chem.* **2013**, *11*, 6929–6933.

[13] F. G. Mutti, C. S. Fuchs, D. Pressnitz, J. H. Sattler, W. Kroutil, *Adv. Synth. Catal.* **2011**, *353*, 3227–3233.

[14] a) M. D. Toscano, K. J. Woycechowsky, D. Hilvert, *Angew. Chem.* **2007**, *119*, 3274–3300; *Angew. Chem. Int. Ed.* **2007**, *46*, 3212–3236; b) G. Kiss, N. Çelebi-Ölçüm, R. Moretti, D. Baker, K. N. Houk, *Angew. Chem. Int. Ed.* **2013**, *52*, 5700–5725.

[15] Initial reaction rates per 1 μM enzyme were 227.3, 4.4, 0.5 and 5.6 μM min^{-1} for (*S*)-**1a**–**d**, respectively. Reaction conditions were 50 mM (*S*)-amine and 50 mM pyruvate.

[16] M. Höhne, S. Schätzle, H. Jochens, K. Robins, U. T. Bornscheuer, *Nat. Chem. Biol.* **2010**, *6*, 807–813.

[17] C. Rausch, A. Lerchner, A. Schiefner, A. Skerra, *Proteins: Struct., Funct., Bioinf.* **2013**, *81*, 774–787.

[18] M. S. Humble, K. E. Cassimjee, M. Häkansson, Y. R. Kimbung, B. Walse, V. Abedi, H. J. Federsel, P. Berglund, D. T. Logan, *FEBS J.* **2012**, *279*, 779–792.

[19] F. Steffen-Munsberg, C. Vickers, A. Thontowi, S. Schätzle, T. Tumlirsch, M. Svedendahl Humble, H. Land, P. Berglund, U. T. Bornscheuer, M. Höhne, *ChemCatChem* **2013**, *5*, 150–153.

[20] Initial reaction rates were 0.45 and 1.24 mM min^{-1} for (*S*)-**1a** and benzylamine, respectively. Reaction conditions were 50 mM (*S*)-**1a** or benzylamine, 50 mM pyruvate and 2 μM OATA.

[21] M. T. Reetz, *Angew. Chem.* **2011**, *123*, 144–182; *Angew. Chem. Int. Ed.* **2011**, *50*, 138–174.

[22] C. S. Chen, Y. Fujimoto, G. Girdaukas, C. J. Sih, *J. Am. Chem. Soc.* **1982**, *104*, 7294–7299.

[23] E. S. Park, M. S. Malik, J. Y. Dong, J. S. Shin, *ChemCatChem* **2013**, *5*, 1734–1738.

[24] a) M. Thomsen, L. Skalden, G. J. Palm, M. Höhne, U. T. Bornscheuer, W. Hinrichs, *Acta Crystallogr. Sect. D: Biol. Crystallogr.* **2014**, *70*, 1086–1093; b) A. Lyskowski, C. Gruber, G. Steinkellner, M. Schürmann, H. Schwab, K. Gruber, K. Steiner, *PLoS ONE* **2014**, *9*, e87350.

[25] E. S. Park, J. Y. Dong, J. S. Shin, *ChemCatChem* **2013**, *5*, 3538–3542.

[26] E. S. Park, M. Kim, J. S. Shin, *Appl. Microbiol. Biotechnol.* **2012**, *93*, 2425–2435.

[27] E. S. Park, J. S. Shin, *Appl. Environ. Microbiol.* **2013**, *79*, 4141–4144.

[28] a) C. B′Hymer, M. Montes-Bayon, J. A. Caruso, *J. Sep. Sci.* **2003**, *26*, 7–19; b) R. Bhushan, H. Brückner, *Amino Acids* **2004**, *27*, 231–247.

